

Reducing the nucleation barrier in magnetocaloric Heusler alloys by nanoindentation

R. Niemann, S. Hahn, A. Diestel, A. Backen, L. Schultz, K. Nielsch, M. F.-X. Wagner, and S. Fähler

Citation: *APL Materials* **4**, 064101 (2016); doi: 10.1063/1.4943289

View online: <https://doi.org/10.1063/1.4943289>

View Table of Contents: <http://aip.scitation.org/toc/apm/4/6>

Published by the [American Institute of Physics](#)

Articles you may be interested in

[Large reversible magnetocaloric effect in Ni-Mn-In-Co](#)

Applied Physics Letters **106**, 021901 (2015); 10.1063/1.4905371

[Field-temperature phase diagrams of freestanding and substrate-constrained epitaxial Ni-Mn-Ga-Co films for magnetocaloric applications](#)

Journal of Applied Physics **118**, 023908 (2015); 10.1063/1.4922358

[Large magnetic-field-induced strains in Ni₂MnGa single crystals](#)

Applied Physics Letters **69**, 1966 (1996); 10.1063/1.117637

[Advanced materials for magnetic cooling: Fundamentals and practical aspects](#)

Applied Physics Reviews **4**, 021305 (2017); 10.1063/1.4983612

[Reversibility of minor hysteresis loops in magnetocaloric Heusler alloys](#)

Applied Physics Letters **110**, 223904 (2017); 10.1063/1.4984797

[Magnetocaloric effect in the low hysteresis Ni-Mn-In metamagnetic shape-memory Heusler alloy](#)

Journal of Applied Physics **115**, 173907 (2014); 10.1063/1.4874935

PHYSICS TODAY

WHITEPAPERS

ADVANCED LIGHT CURE ADHESIVES

Take a closer look at what these environmentally friendly adhesive systems can do

READ NOW

PRESENTED BY
 MASTERBOND
ADHESIVES | SEALANTS | COATINGS

Reducing the nucleation barrier in magnetocaloric Heusler alloys by nanoindentation

R. Niemann,^{1,2,a} S. Hahn,³ A. Diestel,¹ A. Backen,^{1,b} L. Schultz,^{1,2}
K. Nielsch,¹ M. F.-X. Wagner,³ and S. Fähler^{1,2}

¹*IFW Dresden, P.O. Box 270116, D-01171 Dresden, Germany*

²*Department of Physics, Institute for Solid State Physics, Technische Universität Dresden, D-01062 Dresden, Germany*

³*Institute of Materials Science and Engineering, Technische Universität Chemnitz, D-09107 Chemnitz, Germany*

(Received 17 December 2015; accepted 22 February 2016; published online 9 March 2016)

Magnetocaloric materials are promising as solid state refrigerants for more efficient and environmentally friendly cooling devices. The highest effects have been observed in materials that exhibit a first-order phase transition. These transformations proceed by nucleation and growth which lead to a hysteresis. Such irreversible processes are undesired since they heat up the material and reduce the efficiency of any cooling application. In this article, we demonstrate an approach to decrease the hysteresis by locally changing the nucleation barrier. We created artificial nucleation sites and analyzed the nucleation and growth processes in their proximity. We use Ni-Mn-Ga, a shape memory alloy that exhibits a martensitic transformation. Epitaxial films serve as a model system, but their high surface-to-volume ratio also allows for a fast heat transfer which is beneficial for a magnetocaloric regenerator geometry. Nanoindentation is used to create a well-defined defect. We quantify the austenite phase fraction in its proximity as a function of temperature which allows us to determine the influence of the defect on the transformation. © 2016 Author(s). All article content, except where otherwise noted, is licensed under a Creative Commons Attribution (CC BY) license (<http://creativecommons.org/licenses/by/4.0/>). [<http://dx.doi.org/10.1063/1.4943289>]

Magnetocaloric materials are interesting for future cooling applications.¹ Most compounds that are currently discussed, including La-Fe-Si,² MnAs,³ Mn-Fe-P,⁴ and the Heusler compounds⁵ Ni-Mn-X (X = Al⁶, In⁷, Sn,⁸ Sb⁹), which are isostructural to Ni-Mn-Ga,¹⁰ show a giant magnetocaloric effect due to a first-order phase transition that can be induced by an external magnetic field.¹¹ The latent heat of the transformation is then used in a cooling cycle. However, a drawback of all first-order materials is the hysteresis. Irreversible processes heat up the material, which reduces the cooling efficiency¹ and also diminishes the performance in heat pumps.¹²

Hysteresis in first-order transitions is a consequence of the formation and movement of phase boundaries. This leads to energy barriers that have to be overcome to form a nucleus and grow the product phase. In order to reduce the energy barriers and thus the hysteresis in magnetocaloric applications, different approaches have been proposed which are either structure- or microstructure-related. Approaches tackling the structure try to decrease the lattice misfit between both phases at the phase boundary. This can be achieved by reducing the volume change and, in symmetry breaking transitions, by additionally fulfilling well-defined boundary conditions for the lattice constants.¹³ Both can be achieved by tuning the chemical composition,¹⁴ but this commonly also changes other important intrinsic parameters like the transformation temperature or magnetization difference which directly influence the magnetocaloric effect. Microstructural approaches usually

^aAuthor to whom correspondence should be addressed. Electronic mail: r.niemann@ifw-dresden.de

^bNow at CNRS, Grenoble, France.

try to decrease the nucleation barrier. In general, these barriers are drastically reduced close to defects, where heterogeneous nucleation is possible. Consequently, the hysteresis can be effectively reduced by introducing defects via ion irradiation, which was shown recently for Mn-As-based compounds.¹⁵ The nucleation is favoured near precipitates consisting of a non-transforming phase.¹⁶ In Heusler alloys, it is also possible to use a thermodynamic cycle within minor loops of the hysteresis, which preserves a certain fraction of both phases and enhances the reversibility significantly.¹⁷ For the martensitic Heusler alloys, the direct transformation during cooling represents the main challenge since the reverse transformation proceeds more continuously because residual austenite is present also at very low temperatures.¹⁸

In this article, a microstructure-based approach is used to demonstrate that the nucleation barrier can be decreased in the vicinity of a remanent indent. The radius of influence of this defect is quantified from *in situ* observations of the nucleation and growth of martensite in a scanning electron microscope. Finally, a way to realize this process also on a macroscopic scale is discussed.

As a model system, epitaxial films of the Heusler alloy Ni-Mn-Ga are used. Ni-Mn-Ga is a magnetic shape memory alloy that exhibits a ferroelastic (martensitic) transformation from a high-temperature cubic austenite phase into a low-temperature martensite phase with lower symmetry. Depending on the composition, this transformation can be tuned to take place near room temperature. This compound shows a small magnetocaloric effect¹⁰ but is identical in structure and microstructure to some giant magnetocaloric compounds, e.g., Ni-Mn-In and therefore a suitable model system. Then, modulated phases are observed in the martensitic state, often approximately described by a monoclinic or orthorhombic unit cell.¹⁹ Due to the differences in spontaneous magnetization, magnetic and elastic anisotropy, and tetragonality between austenite and martensite,²⁰ the transformation can be induced by both magnetic and elastic fields.^{21,22} Accordingly, the transformation is also extremely sensitive to mechanical stresses^{23,24} and therefore strongly influenced by the elastic stray fields of defects. The martensitic transformation was, e.g., triggered by nanoindentation on shape memory films in the austenitic state.^{25,26}

For a microstructure-based approach, it is necessary to understand the martensitic microstructure, which has been examined in detail for this material, since it shows giant reversible strains when subjected to magnetic fields.^{27,28} This effect is influenced by the type and arrangement of twin boundaries.²⁹ The hysteresis in these materials depends critically on the microstructure that forms during the martensitic transformation. Usually, a complex hierarchy of twins-within-twins separated by twin boundaries on many length scales is observed.^{30–32} This microstructure can be understood by analyzing how it is formed: the first-order transformation sets off with nucleation of the modulated phase which can also be described as nano-twinned.^{31,33,34} Then the phase grows with well-defined growth modes^{18,35} and forms macroscale twin boundaries in a final coalescence step.³⁶ The symmetry of the final microstructure is constrained by the symmetry of both phases, but the actual distribution of twin boundaries is determined by the kinetics of the transformation.

A 1.5 μm thick epitaxial $\text{Ni}_{48.4}\text{Mn}_{32.8}\text{Ga}_{18.8}$ film was produced by sputter deposition onto the (100)-face of a heated single crystalline MgO substrate; details about film deposition are published elsewhere.³⁷ Before depositing the film, an epitaxial chromium layer with a thickness of 100 nm was grown to promote epitaxy. By reciprocal space mapping (RSM) at room temperature (not shown), it was determined that the Ni-Mn-Ga film has the structure of a modulated 14M phase with lattice constants $a = 0.616$ nm, $b = 0.579$ nm, $c = 0.554$ nm, and $\gamma = 90.4^\circ$ (using a monoclinic cell derived from the $L2_1$ cubic cell^{19,29}). Temperature-dependent RSM showed that the film undergoes a martensitic transformation at around 400 K. Electron micrographs were acquired using a Zeiss LEO 1530 Gemini microscope equipped with a back-scattered electron (BSE) detector and an electron back-scatter diffraction (EBSD) setup which includes an additional detector for forward-scattered electrons (FSE). EBSD patterns were indexed using an orthorhombic cell, as due to the high twin boundary density, an unambiguous indexing with a monoclinic cell was not possible. All crystal planes and directions in this article are given with respect to the cubic austenite cell. Inside the SEM, the sample was heated by a Kammerath and Weiss sample stage that allows for temperature steps of 1 K. The temperature was varied in a range from room temperature up to 423 K. Atomic force microscopy was performed using a Digital Instruments' DI 3100 in tapping mode.

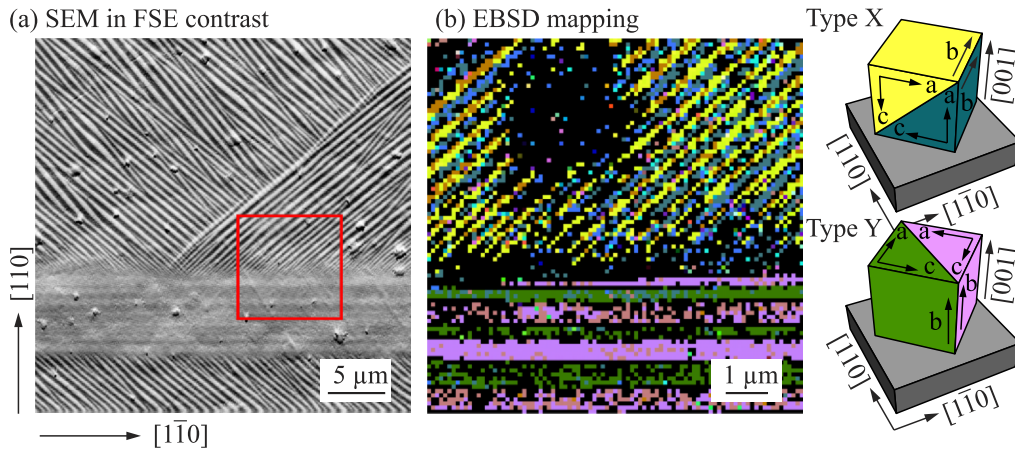


FIG. 1. (a) SEM micrograph of the typical microstructure of an epitaxial Ni-Mn-Ga film in the martensitic state. (b) EBSD mapping of the area that is marked in red in (a). An orthorhombic unit cell was used for indexing. The two different microstructures that can be identified are sketched in the legend: type X has the b -axis in the film plane and c - a -twin boundaries oriented by approximately 45° to the film normal. In type Y, the b -axis and the c - a -twin boundaries are aligned perpendicular to the film plane.

To analyze the martensitic microstructure of a Ni-Mn-Ga film, an electron micrograph and an EBSD mapping were acquired (Fig. 1). Two types of microstructures can be distinguished already in the FSE image. The EBSD mapping shows that the differences between both microstructures are the orientation of the crystallographic axes and hence also the twin boundary orientation. The “type X” microstructure,^{36,38} also called “high contrast zone” because of the pronounced topographic contrast at the twin boundaries,³⁹ consists of martensitic 14M variants having their b -axis in the film plane. These variants are separated by c - a -twin boundaries that coincide with the crystallographic (011) , $(0\bar{1}\bar{1})$, (101) , or $(10\bar{1})$ planes and are inclined by 45° relative to the substrate normal. The twin boundary traces at the film surface are oriented along $\langle 100 \rangle$ directions and hence along the diagonals of the SEM images. The second type of microstructure, “type Y”^{36,38} or “low contrast zone,”³⁹ has the b -axis of all martensitic variants out of plane. The twin boundaries are also c - a -twin boundaries that coincide with (110) or $(\bar{1}\bar{1}0)$ planes which are perpendicular to the film plane. The traces of these twin boundaries at the surface are parallel to the $\langle 110 \rangle$ -oriented picture edges.

To create a permanent surface defect, nanoindentation was performed at room temperature in the martensitic state using a nanomechanical tester by ASMEC with a pyramidal Berkovich tip and a maximum force of 20 mN. The plastically deformed surface area close to the remanent indent was analyzed at room temperature by atomic force microscopy (Fig. 2(a)). The tip has left a regular triangular indent with an edge length of about $1 \mu\text{m}$. Additional topography from the martensitic microstructure is visible.

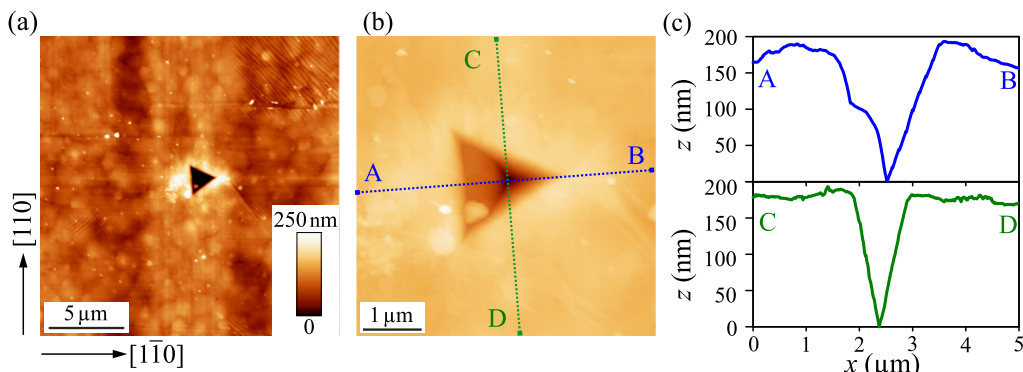


FIG. 2. AFM images of the remanent indent. Additional topography from the martensitic microstructure is visible. (a) At larger scale, (b) in a close-up, and (c) height z along the profiles A-B and C-D.

the vicinity of the indent is caused by the martensitic microstructure. The contrast appears weak since the height variations due to twinning are much smaller than the depth of the indent. Fig. 2(b) shows an atomic force image with higher resolution close to the indent to analyze finer structures. We observe a pile-up of material around the indent, which is typical for plastic deformation.⁴⁰ Fig. 2(c) shows profile plots along perpendicular lines through the center of the indent with a depth of about 170 nm. Its shape is not perfectly pyramidal; there is a kink in the left face of the indent. This additional deformation could be due to the (pseudo-)plastic anisotropy of Ni-Mn-Ga⁴¹ in combination with the three-fold symmetry of the tip, which deviates from the four-fold symmetry of the epitaxial film. Due to the geometry of the self-similar indenter tip, the representative strain below the tip is 8%, independent of the applied load or indentation depth.^{40,42} We showed above that the martensite was in a multi-variant state before the indentation, hence the maximum strain that could possibly be mediated by twin boundary movement amounts to about $\frac{2c}{a+c} - 1 = -5.3\%$. The actual value will be much smaller due to the orientation distribution of the twin boundaries. This means that the deformation near the indent was mostly plastic by movement of dislocations and not entirely pseudo-plastic by twin boundary movement. The latter is additionally hindered by the complex hierarchical arrangement of twin boundaries.³⁶

To determine how the indent influences the martensitic transformation on a local scale, a series of scanning electron micrographs was acquired during the martensitic transformation. At this point, the sample had already undergone 5 martensitic transformations for other studies. Before each image, the temperature was kept stable for 15 min, hence every image depicts a metastable state. A selection of images is shown in Fig. 3. A video containing all images taken can be found in the supplementary material.⁴³ Fig. 3(a) shows the martensitic microstructure around the indent at 353 K. The microstructure consists of type X (diagonal features) and type Y (horizontal and vertical features). Above the transformation temperature, at 423 K (Fig. 3(b)), the film is almost entirely in the austenitic state except for a few remanent type Y “needles” that are preserved very close to the indent. After cooling the sample to 408 K (Fig. 3(c)), these needles grow away from the indent and hence the phase fraction of martensite very close to the indent is increased. The rest of the observed sample remains in the austenitic phase. Upon further cooling to 404 K, the needles close to the indent grow further along [110]. Additionally, a martensitic needle along the [100] direction forms directly at the indent (red arrow). Near the right edge of the image, a new group of type Y needles forms which is not directly connected to the indent. It may have nucleated independently

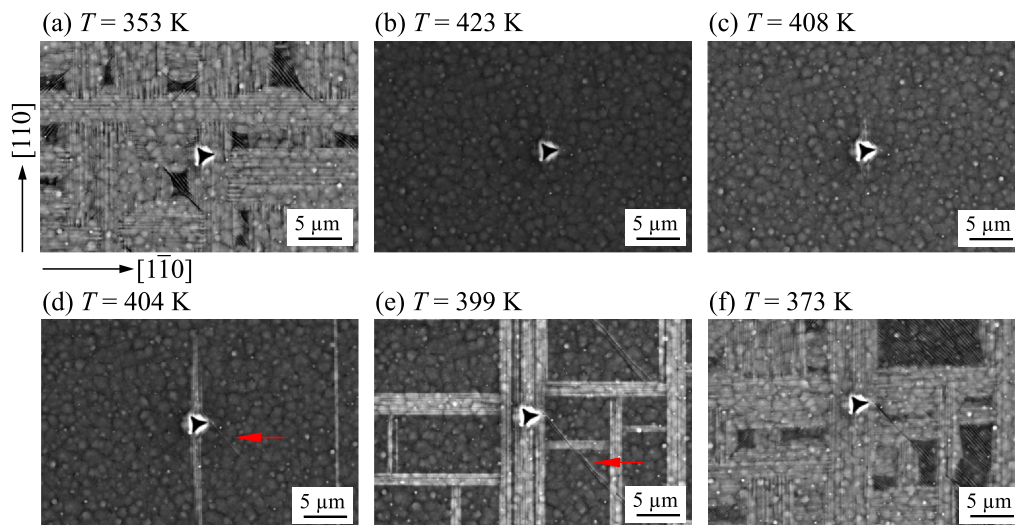


FIG. 3. SEM micrographs in back scattered electron contrast reveal the martensitic microstructure near the indent at different temperatures. (a) The microstructure after indentation. (b) After heating, the sample becomes austenitic. (c) and (d) Upon cooling, the martensitic transformation starts at the indent by formation of type Y martensite and a separate type X needle (red arrow). (e) The martensite grows further until (f) a final, different microstructure is reached.

at another defect or due to some long-range elastic stray field of the indent. At 399 K, we observe an increased fraction of type Y martensite. The central group of needles near the indent has thickened and additional needles that are oriented along the $[1\bar{1}0]$ direction have formed. Those cannot grow across existing martensite. Finally, at 373 K, almost the entire sample is in the martensitic state. The microstructure again consists only of type X and Y elements but the particular pattern is significantly different compared to the original martensitic microstructure from Fig. 3(a). Only near the indent, the type and orientation of the martensite (type Y along $[110]$) were preserved. This illustrates that the transformation path is very sensitive to small variations in the boundary conditions.

To quantify the effect of the indent on the transformation, the series of electron micrographs was further evaluated: the phase fractions were determined by measuring the surface area covered by austenite and martensite, respectively (Fig. 4). By processing all images from the temperature series, this analysis yields an approximation of the phase fraction as a function of temperature. To identify the radius of influence of the indent, we defined a cut-off radius r . The quantitative evaluation of the phase fraction was then performed separately for the surface area lying within and outside the cut-off radius, respectively (Fig. 4(a)). The cut-off radius was varied between $1\ \mu\text{m}$ and $12\ \mu\text{m}$. These limits are given by the size of the indent and of the observed area, respectively.

As a result of this evaluation, the temperature dependence of the austenite phase fraction is plotted exemplarily for $r = 2\ \mu\text{m}$ in Fig. 4(b). Inside the radius of $2\ \mu\text{m}$, the phase fraction of austenite starts to decrease already at around 410 K while outside the radius, the austenite is stable until 400 K. This is obviously a consequence of the martensite growing first near the indent. During further cooling, the austenite phase fraction far from the indent lags behind the austenite fraction inside the radius. In Fig. 4(c), the phase fraction is plotted for a radius of $6\ \mu\text{m}$. In this case, there is almost no difference between the transformation outside and inside the radius. Apart from little deviations near the beginning of the transformation, no significant difference can be observed.

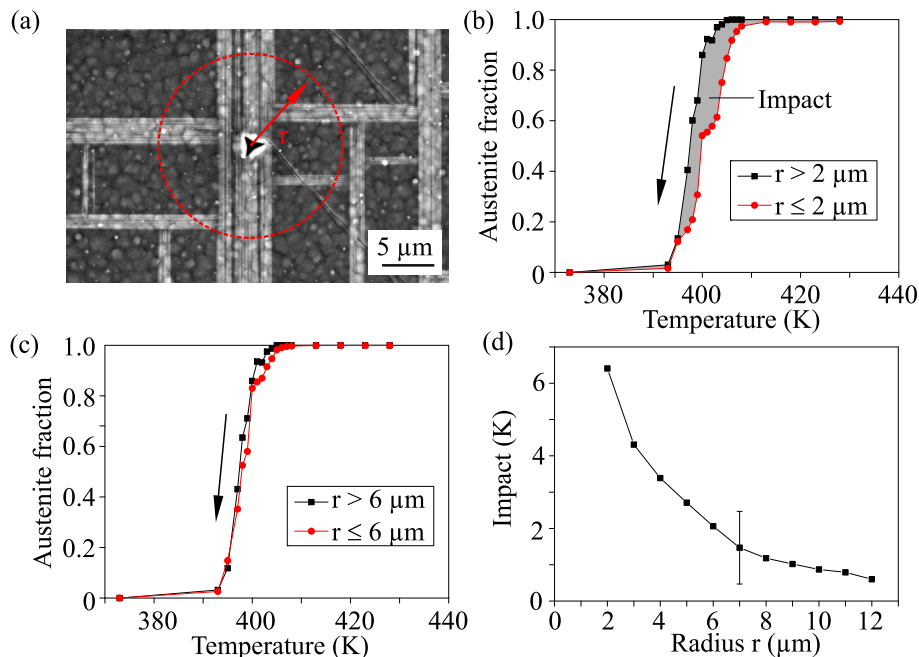


FIG. 4. Quantification of the impact of an indent measured for decreasing temperature. (a) Microstructure near the remanent indent during the martensitic transformation. A critical radius around the indent is defined. The dependence of the fraction of austenite inside (red) and outside (black) a cut-off radius of (b) $2\ \mu\text{m}$ and (c) $6\ \mu\text{m}$ around the remanent indent is shown. The fraction was calculated by measuring the surface fraction of both phases. (d) The integral of the difference between the phase fraction inside and outside the radius is called impact (gray area in (b)) and is a measure for the influence of the indent for any given radius. (d) shows the dependency of the impact on the radius. For radii smaller than $6\ \mu\text{m}$, a significant influence is observed.

The “impact” of the indent is quantified by a single number from an integration of the difference between the phase fraction inside and outside the radius. This area is highlighted in gray in Fig. 4(b). The radius of influence around an indent is achieved by plotting the impact as a function of r (Fig. 4(d)). The impact monotonously decays with increasing radius, which is expected since the influence should vanish at large distances. From these measurements, we can conclude that one indent controls nucleation within a radius of about $6\ \mu\text{m}$. This is significantly larger than the indent itself, illustrating that nanoindentation is an effective way to control nucleation. However, the affected radius is still in the order of the film thickness of $1.5\ \mu\text{m}$, indicating that the influence radius is mostly limited by clamping of the film to the rigid substrate.

The present work demonstrates that an indent can promote the martensitic transformation on a local scale. The well defined experiment allows for a better understanding of the observation that martensite usually starts to grow, e.g., near scratches at the surface of a sample.⁴⁴ We suggest that the underlying mechanism is the increase of the temperature at which the transformation takes place in vicinity of a plastic deformation due to its elastic stray field. This leads to a relative shift of the respective free energy curves of both phases and results in a stress induced martensite.⁴⁵ Due to the local increase of the temperature at which the transformation takes place, this martensite will nucleate first.

Our observation is that one indent does not result in a switching of the entire sample but only predominantly affects the transformation in a radius of the order of less than $10\ \mu\text{m}$, which suggests that the latter mechanism is more important.

In the film-shaped sample we used, the effect is limited to a small area around each indent. To influence the transformation on a macroscopic scale, the indents could be placed preferably in a hexagonal lattice and with a lattice constant in the order of several μm , which corresponds to a density in the order of $\approx 10^{10}\ \text{m}^{-2}$. A technology to create an array of indents was proposed in the framework of micromechanical memory, the “millipede.”⁴⁶ It never found application in computer technology, but in the fabrication of an array of defects, this appears to be a promising approach to make magnetocaloric thin films ready for applications. In a bulk process, we propose to add defects, e.g., by precipitation reactions or adding inert microparticles. As the transformation proceeds by nucleation and growth, one should optimize defect size and distribution not only with respect to their nucleation ability but also for a minimized pinning potential.

The authors thank S. Schwabe, B. Schleicher, and S. Kauffmann-Weiss for helpful discussions. R.N., A.D., and S.F. gratefully acknowledge funding by DFG via No. SPP1599, www.ferroiccooling.de.

- ¹ S. Fähler, U. K. Röbler, O. Kastner, J. Eckert, G. Eggeler, H. Emmerich, P. Entel, S. Müller, E. Quandt, and K. Albe, “Caloric effects in ferroic materials: New concepts for cooling,” *Adv. Eng. Mater.* **14**, 10–19 (2012).
- ² E. Lovell, A. M. Pereira, A. D. Caplin, J. Lyubina, and L. F. Cohen, “Dynamics of the first-order metamagnetic transition in magnetocaloric La(Fe,Si)(13): Reducing hysteresis,” *Adv. Energy Mater.* **5**, 1401639 (2015).
- ³ N. K. Sun, W. B. Cui, D. Li, D. Y. Geng, F. Yang, and Z. D. Zhang, “Giant room-temperature magnetocaloric effect in Mn(1-x)Cr(x)As,” *Appl. Phys. Lett.* **92**, 072504 (2008).
- ⁴ V. Basso, M. Kupferling, C. Curcio, C. Bennati, A. Barzca, M. Katter, M. Bratko, E. Lovell, J. Turcaud, and L. F. Cohen, “Specific heat and entropy change at the first order phase transition of La(Fe-Mn-Si)(13)-H compounds,” *J. Appl. Phys.* **118**, 053907 (2015).
- ⁵ A. Planes, L. Manosa, and M. Acet, “Magnetocaloric effect and its relation to shape-memory properties in ferromagnetic heusler alloys,” *J. Phys.: Condens. Matter* **21**, 233201 (2009).
- ⁶ H. Xuan, F. Chen, P. Han, D. Wang, and Y. Du, “Effect of Co addition on the martensitic transformation and magnetocaloric effect of Ni-Mn-Al ferromagnetic shape memory alloys,” *Intermetallics* **47**, 31–35 (2014).
- ⁷ T. Krenke, M. Acet, E. F. Wassermann, X. Moya, L. Mañosa, and A. Planes, “Martensitic transitions and the nature of ferromagnetism in the austenitic and martensitic states of Ni-Mn-Sn alloys,” *Phys. Rev. B* **72**, 014412 (2005).
- ⁸ T. Krenke, E. Duman, M. Acet, E. Wassermann, X. Moya, L. Manosa, and A. Planes, “Inverse magnetocaloric effect in ferromagnetic Ni-Mn-Sn alloys,” *Nat. Mater.* **4**, 450 (2005).
- ⁹ A. K. Nayak, K. G. Suresh, and A. K. Nigam, “Giant inverse magnetocaloric effect near room temperature in Co substituted nimsb heusler alloys,” *J. Phys. D: Appl. Phys.* **42**, 035009 (2009).
- ¹⁰ A. Aliev, A. Batdalov, S. Bosko, V. Buchelnikov, I. Dikshtein, V. Khovailo, V. Koledov, R. Levitin, V. Shavrov, and T. Takagi, “Magnetocaloric effect and magnetization in a Ni-Mn-Ga heusler alloy in the vicinity of magnetostructural transition,” *J. Magn. Magn. Mater.* **272-276**, 2040–2042 (2004).
- ¹¹ V. K. Pecharsky and K. A. Gschneidner, “Giant magnetocaloric effect in Gd₅(Si₂Ge₂),” *Phys. Rev. Lett.* **78**, 4494–4497 (1997).
- ¹² C. Bahl, “Developing a magnetocaloric domestic heat pump,” in *Proceedings of the 6th IIF-IIR International Conference on Magnetic Refrigeration (IIF-IIR, 2014)*.

- ¹³ Y. Zhang, R. Hughes, J. Britten, W. Gong, J. Preston, G. Botton, and M. Niewczas, "Epitaxial Ni–Mn–Ga films derived through high temperature *in situ* depositions," *Smart Mater. Struct.* **18**, 025019 (2009).
- ¹⁴ J. Cui, Y. S. Chu, O. O. Famodu, Y. Furuya, J. Hatrick-Simpers, R. D. James, A. Ludwig, S. Thienhaus, M. Wuttig, Z. Zhang, and I. Takeuchi, "Combinatorial search of thermoelastic shape-memory alloys with extremely small hysteresis width," *Nat. Mater.* **5**, 286–290 (2006).
- ¹⁵ M. Trassinelli, M. Marangolo, M. Eddrief, V. H. Etgens, V. Gafton, S. Hidki, E. Lacaze, E. Lamour, C. Prigent, J.-P. Rozet, S. Steydli, Y. Zheng, and D. Vernhet, "Suppression of the thermal hysteresis in magnetocaloric MnAs thin film by highly charged ion bombardment," *Appl. Phys. Lett.* **104**, 081906 (2014).
- ¹⁶ N. Zhou, C. Shen, M. F.-X. Wagner, G. Eggeler, M. J. Mills, and Y. Wang, "Effect of Ni₄Ti₃ precipitation on martensitic transformation in Ti–Ni," *Acta Mater.* **58**, 6685–6694 (2010).
- ¹⁷ T. Gottschall, K. Skokov, B. Frincu, and O. Gutfleisch, "Large reversible magnetocaloric effect in Ni–Mn–In–Co," *Appl. Phys. Lett.* **106**, 021901 (2015).
- ¹⁸ A. Diestel, R. Niemann, B. Schleicher, L. Schultz, and S. Fähler, "Field-temperature phase diagrams of freestanding and substrate-constrained epitaxial Ni–Mn–Ga–Co films for magnetocaloric applications," *J. Appl. Phys.* **118**, 023908 (2015).
- ¹⁹ J. Pons, V. Chernenko, R. Santamarta, and E. Cesari, "Crystal structure of martensitic phases in Ni–Mn–Ga shape memory alloys," *Acta Mater.* **48**, 3027 (2000).
- ²⁰ P. Klaer, H. C. Herper, P. Entel, R. Niemann, L. Schultz, S. Faehler, and H. J. Elmers, "Electronic structure of the austenitic and martensitic state of magnetocaloric Ni–Mn–In heusler alloy films," *Phys. Rev. B* **88**, 174414 (2013).
- ²¹ V. Chernenko, V. L'vov, J. Pons, and E. Cesari, "Superelasticity in high-temperature Ni–Mn–Ga alloys," *J. Appl. Phys.* **93**, 2394 (2003).
- ²² O. Heczko, M. Thomas, R. Niemann, L. Schultz, and S. Fähler, "Magnetically induced martensite transition in freestanding epitaxial Ni–Mn–Ga films," *Appl. Phys. Lett.* **94**, 152513 (2009).
- ²³ V. Chernenko, J. Pons, E. Cesari, and K. Ishikawa, "Stress-temperature phase diagram of a ferromagnetic Ni–Mn–Ga shape memory alloy," *Acta Mater.* **53**, 5071 (2005).
- ²⁴ R. Niemann, J. Baro, O. Heczko, L. Schultz, S. Fähler, E. Vives, L. Manosa, and A. Planes, "Tuning avalanche criticality: Acoustic emission during the martensitic transformation of a compressed Ni–Mn–Ga single crystal," *Phys. Rev. B* **86**, 214101 (2012).
- ²⁵ X. G. Ma and K. Komvopoulos, "*In situ* transmission electron microscopy and nanoindentation studies of phase transformation and pseudoelasticity of shape-memory titanium-nickel films," *J. Mater. Res.* **20**, 1808–1813 (2005).
- ²⁶ Y. Liu, I. Karaman, H. Wang, and X. Zhang, "Two types of martensitic phase transformations in magnetic shape memory alloys by *in-situ* nanoindentation studies," *Adv. Mater.* **26**, 3893–3898 (2014).
- ²⁷ K. Ullakko, J. Huang, C. Kantner, R. O'Handley, and V. Kokorin, "Large magnetic-field-induced strains in Ni₂MnGa single crystals," *Appl. Phys. Lett.* **69**, 1966 (1996).
- ²⁸ A. Sozinov, N. Lanska, A. Soroka, and W. Zou, "12% magnetic field-induced strain in Ni–Mn–Ga-based non-modulated martensite," *Appl. Phys. Lett.* **102**, 021902 (2013).
- ²⁹ L. Straka, H. Hänninen, and O. Heczko, "Temperature dependence of single twin boundary motion in Ni–Mn–Ga martensite," *Appl. Phys. Lett.* **98**, 141902 (2011).
- ³⁰ A. Roytburd, "Elastic domains and polydomain phases in solids," *Phase Transitions* **45**, 1 (1993).
- ³¹ S. Kaufmann, R. Niemann, T. Thersleff, U. Röbber, O. Heczko, J. Buschbeck, B. Holzapfel, L. Schultz, and S. Fähler, "Modulated martensite: Why it forms and why it deforms easily," *New J. Phys.* **13**, 053029 (2011).
- ³² S. Kaufmann, U. Röbber, O. Heczko, M. Wuttig, J. Buschbeck, L. Schultz, and S. Fähler, "Adaptive modulations of martensites," *Phys. Rev. Lett.* **104**, 145702 (2010).
- ³³ A. Khachatryan, S. Shapiro, and S. Semenovskaya, "Adaptive phase formation in martensitic transformation," *Phys. Rev. B* **43**, 10832 (1991).
- ³⁴ R. Niemann, U. K. Röbber, M. E. Gruner, O. Heczko, L. Schultz, and S. Fähler, "The role of adaptive martensite in magnetic shape memory alloys," *Adv. Eng. Mater.* **14**, 562–581 (2012).
- ³⁵ Z. Li, "Study on crystallographic features of Ni–Mn–Ga ferromagnetic shape memory alloys," Ph.D. dissertation, Université de Lorraine and Northeastern University, 2011.
- ³⁶ A. Backen, S. Kauffmann-Weiss, C. Behler, A. Diestel, R. Niemann, A. Kauffmann, J. Freudenberger, L. Schultz, and S. Fähler, "Mesoscopic twin boundaries in epitaxial Ni–Mn–Ga films," e-print [arXiv:1311.5428](https://arxiv.org/abs/1311.5428) [cond-mat.mtrl-sci] (2013).
- ³⁷ A. Backen, S. Yeduru, M. Kohl, S. Baunack, A. Diestel, B. Holzapfel, L. Schultz, and S. Fähler, "Comparing properties of substrate-constrained and freestanding epitaxial Ni–Mn–Ga films," *Acta Mater.* **58**, 3415 (2010).
- ³⁸ P. Ranzieri, M. Campanini, S. Fabbri, L. Nasi, F. Casoli, R. Cabassi, E. Buffagni, V. Grillo, C. Magen, F. Celegato, G. Barrera, P. Tiberto, and F. Albertini, "Achieving giant magnetically induced reorientation of martensitic variants in magnetic shape-memory Ni–Mn–Ga films by microstructure engineering," *Adv. Mater.* **27**, 4760–4766 (2015).
- ³⁹ B. Yang, Z. B. Li, Y. D. Zhang, G. W. Qin, C. Esling, O. Perroud, X. Zhao, and L. Zuo, "Microstructural features and orientation correlations of non-modulated martensite in Ni–Mn–Ga epitaxial thin films," *Acta Mater.* **61**, 6809–6820 (2013).
- ⁴⁰ A. C. Fischer-Cripps, *Nanoindentation* (Springer, 2002).
- ⁴¹ A. M. Jakob, M. Müller, B. Rauschenbach, and S. G. Mayr, "Nanoscale mechanical surface properties of single crystalline martensitic Ni–Mn–Ga ferromagnetic shape memory alloys," *New J. Phys.* **14**, 033029 (2012).
- ⁴² D. Tabor, "The physical meaning of indentation and scratch hardness," *Br. J. Appl. Phys.* **7**, 159–166 (1956).
- ⁴³ See supplementary material at <http://dx.doi.org/10.1063/1.4943289> for an animation of the entire transformation.
- ⁴⁴ A. G. Khachatryan, *Theory of Structural Transformation in Solids* (John Wiley & Sons, Inc., New York, 1983).
- ⁴⁵ H. E. Karaca, I. Karaman, B. Basaran, D. C. Lagoudas, Y. I. Chumlyakov, and H. J. Maier, *Acta Mater.* **55**, 4253 (2007).
- ⁴⁶ P. Vettiger, G. Cross, M. Despont, U. Drechsler, U. Durig, B. Gotsmann, W. Haberle, M. A. Lantz, H. E. Rothuizen, R. Stutz, and G. K. Binnig, "The 'millipede' - nanotechnology entering data storage," *IEEE Trans. Nanotechnol.* **1**, 39–55 (2002).